

A Mixed-Ligand Approach to a Cobalt-Based Electroactive Framework for Superior Supercapacitor Performance

Safwana Shirin KM,^{a, +} Zahir Abbas,^{a, +} and Shaikh M. Mobin^{*, a, b}

^a Department of Chemistry, Indian Institute of Technology Indore, Simrol, Khandwa Road, Indore 453552, India.

^b Centre for Advanced Electronics (CAE), Indian Institute of Technology Indore, Simrol, Khandwa Road, Indore 453552, India.

*E-mail: xray@iiti.ac.in

Equal contribution

[+] These authors contributed equally to this work

Experimental Section

Materials: 2,3,5,6-tetrafluoro-1,4-benzenedicarboxylic acid (TF, 97%) and Azopyridine (AzPY, 96%) were obtained from Sigma-Aldrich. $\text{Co}(\text{NO}_3)_2 \cdot 6\text{H}_2\text{O}$ (97%), and N,N-dimethylformamide (99.5%) were procured from Merck and SRL Chemicals and used without further purification. Deionized water (DI) was used to prepare electrolytes.

Physical Measurements: Single-crystal analysis was conducted at low temperatures using a CCD-equipped SuperNova diffractometer. Powder X-ray diffraction (PXRD) was performed with Cu $K\alpha$ radiation ($\lambda = 1.5406 \text{ \AA}$) on a Rigaku SmartLab X-ray diffractometer. The FT-IR spectrum, ranging from 4000 to 400 cm^{-1} , was recorded using a Bio-Rad FTS 3000MX instrument with KBr pellets. Thermogravimetric analysis (TGA) was carried out on a METTLER TOLEDO TGA/DSC1 system, employing STARe software at a heating rate of 10 $^\circ\text{C min}^{-1}$ under a nitrogen atmosphere up to 800 $^\circ\text{C}$. Morphological studies were performed using a Supra55 Zeiss field emission scanning electron microscope (FESEM). The BET surface area and pore size distribution were measured using an Autosorb iQ system, version 1.11 (Quantachrome Instruments). X-ray photoelectron spectroscopy (XPS) analyses were conducted with a Thermo Scientific MULTILAB 2000 instrument.

X-ray Crystallography Measurements: Single-crystal X-ray diffraction (SCXRD) data was obtained using a Rigaku Oxford SuperNova CCD diffractometer at 293 K, employing monochromatic graphite Mo $K\alpha$ radiation ($\lambda = 0.71073 \text{ \AA}$). Data acquisition was managed with the CrysAlisPro CCD software, while essential reductions and refinements were carried out using CrysAlisPro RED. The crystal structure was determined using direct methods and further refined with SHELXL-97 by least-squares fitting based on F^2 . All non-hydrogen atoms were refined anisotropically, while hydrogen atoms were placed geometrically and refined with isotropic displacement parameters, typically set at $1.2U_{\text{eq}}$ of their parent atoms.²

Experimental Details:

Synthesis of Co-FLF

Co-FLF was synthesized via a slow diffusion-based crystallization method by dissolving Azopyridine (0.05 mmol) in dimethylformamide (2 mL) and 2,3,5,6-tetrafluoro-1,4-benzenedicarboxylic acid (0.05) in DI water (2 mL). These 2 ligand solutions were mixed and the resulting mixture was stirred for 30 min to form a clear solution. The aqueous solution of (0.1 mmol, 30 mg) $\text{Co}(\text{NO}_3)_2 \cdot 6\text{H}_2\text{O}$ (1 mL) was added into the ligand solution. After the

addition of metal, this solution was kept for 6 days, and reddish crystals were observed to be formed. The crystals were isolated and washed with DMF to ensure high purity.

Electrode Preparation and Electrochemical Measurement

Carbon cloth (CC) was used as the electrode substrate, with 2 M KOH as the electrolyte, to examine the electrochemical performances of Co-FLF and Co-NLF. 1 mg of both electrode materials were taken separately and sonicated in 300 μ L of ethanolic solution. Then, these samples were drop-cast on CC (1×1 cm²) and dried at room temperature. The modified electrodes were used for electrochemical studies performed on an Autolab PGSTAT 204N workstation. The assessments were performed at ambient temperature using a conventional three-electrode setup. Specifically, the electrochemical cell consisted of a platinum wire counter electrode, an Ag/AgCl reference electrode, and a carbon cloth (CC) working electrode. The electrochemical properties of the synthesized Co-FLF and Co-NLF electroactive material were comprehensively evaluated using a trio of key techniques: Cyclic voltammetry (CV), galvanostatic charge-discharge (GCD), and electrochemical impedance spectroscopy (EIS).

Efficiency Evaluation

The electrochemical performance of Co-FLF and Co-NLF were evaluated using galvanostatic charge-discharge (GCD) measurements. The specific capacitance (C_s) was calculated using the following equation:

$$C_s = \frac{I \Delta t}{m \Delta V} \quad (\text{Equation S1})$$

where I/m is the current density, Δt is the discharge time, and ΔV is the potential range of the GCD profile. The specific capacity (Q) of Co-FLF was estimated using the following equation:

$$Q = \frac{I \Delta t}{m} \quad (\text{Equation S2})$$

I/m is the current density, and Δt is the discharge time.

Device Fabrication

We utilized Co-FLF (active material) as the positive electrode, activated carbon as the negative electrode, cellulose paper as the separator, carbon paper (2x4 cm) as the substrate, and 1M KOH/PVA as gel electrolyte for device fabrication. Initially, 5 mg cm⁻² of active material was pasted on carbon paper, and the negative electrode (5 mg cm⁻²) was prepared by mixing

activated carbon and PVDF (85:15) and coating it onto another substrate of carbon paper. The device was assembled with a separator between the positive and negative electrodes. It was then charged using a 300 mAh adapter, and the assembled device successfully powered a commercial LED bulb. The energy density (E) and power density (P) of the asymmetric device (ASC) were determined using the following equations:

$$E = \frac{C_s}{2 \times 3.6} \times \Delta V^2 \quad (\text{Equation S3})$$

$$P = \frac{E}{\Delta t} \times 3600 \quad (\text{Equation S4})$$

where C_s represents the specific capacitance, ΔV is the potential window, and Δt is the discharge time of the GCD profile.

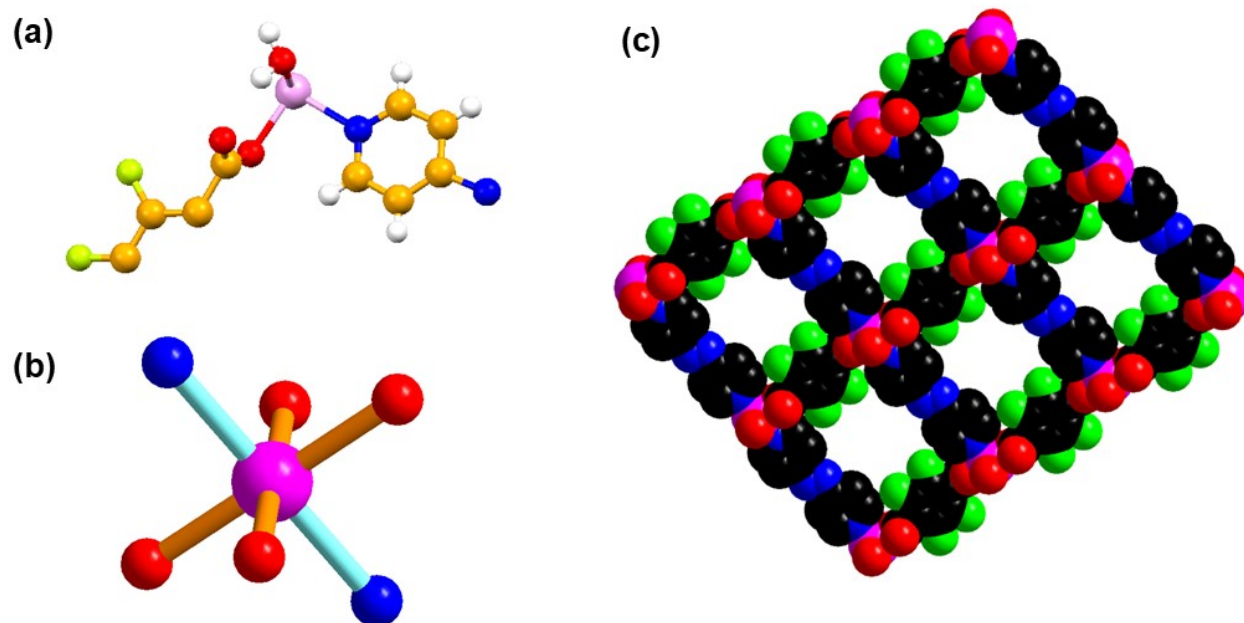


Fig. S1 SCXRD data of Co-FLF (a) asymmetric unit (b) metal coordination geometry (c) Space filling model

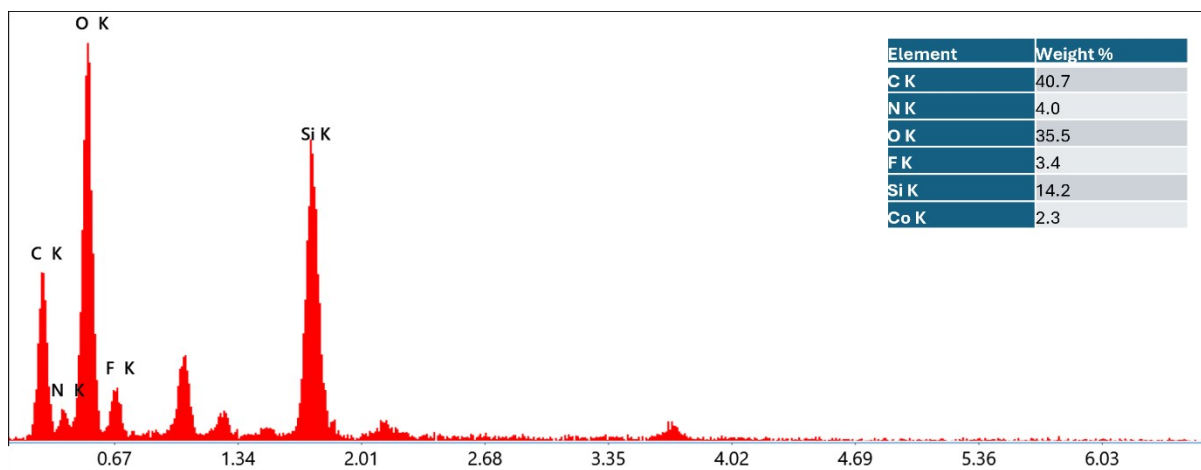


Fig. S2 (a) EDS elemental analysis Co-FLF

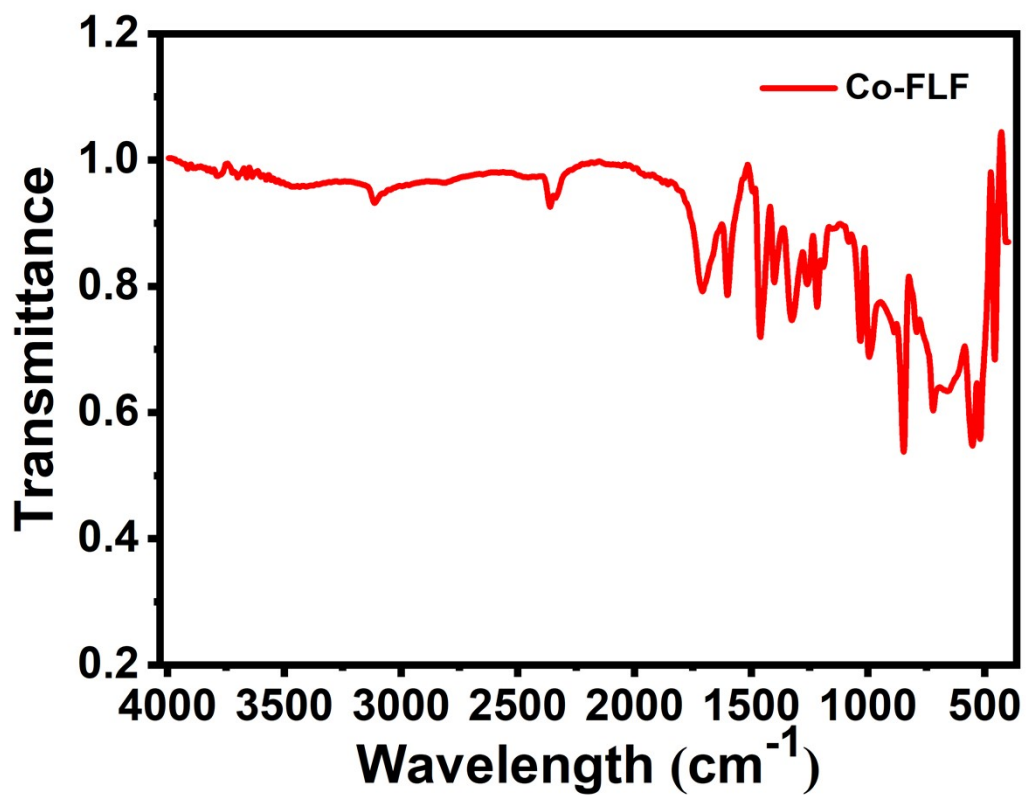


Fig. S3 FT-IR spectra of Co-FLF.

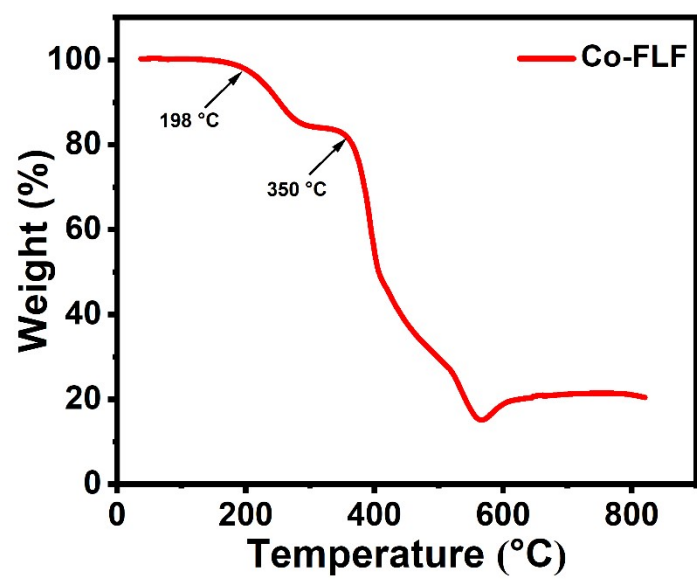


Fig. S4 Thermogravimetric Profile of Co-FLF.

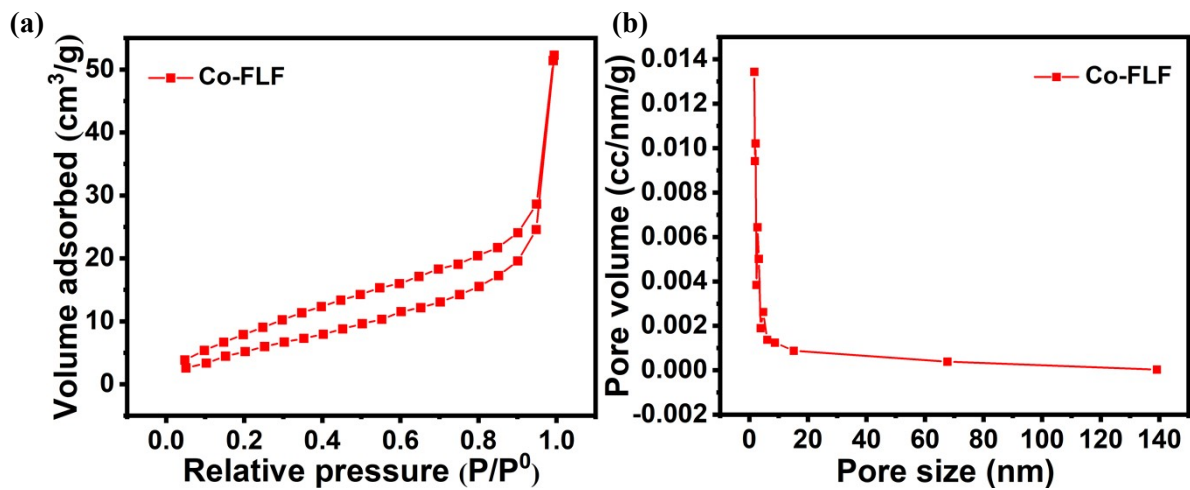


Fig. S5 (a) BET adsorption-desorption isotherm of Co-FLF (b) BJH distribution of Co-FLF.

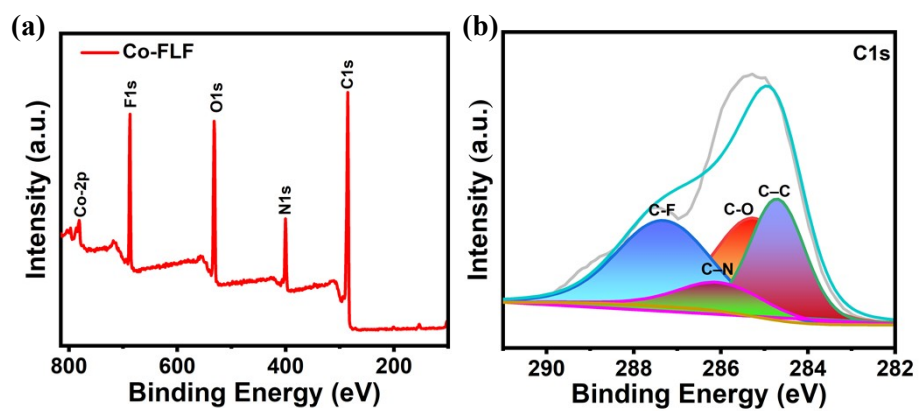
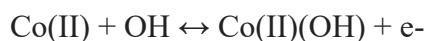


Fig. S6 XPS spectra of Co-FLF (a) Survey Scan, (b) C 1s

Cobalt based layered framework indicated that the redox behavior is predominantly governed by the reversible oxidation of Co(II) centers in the presence of OH⁻ ions from the alkaline electrolyte. This pseudocapacitive behavior is typically attributed to surface or near-surface faradaic reactions involving OH⁻ adsorption, as represented by the following sequential reactions:



These reactions represent a two-step electron transfer process corresponding to the Co(II)/Co(III) redox couple, which plays a crucial role in the pseudocapacitive charge storage mechanism. The porous architecture of the framework further facilitates electrolyte ion diffusion and enhances the accessibility of redox-active sites, thereby improving overall electrochemical performance.³

To elucidate the charge storage mechanism of the Co-FLF electrode materials in KOH electrolyte solution. The relation between cathodic and anodic peaks, and the scan rate (ν) were determined. The b value is calculated for the redox peak.^{4,5}

$$i = a\nu^b \quad (\text{Equation S5})$$

$$\log(i) = b\log(\nu) + \log(a) \quad (\text{Equation S6})$$

Where this parameter represents the scan rate (ν) and the peak current represents (i), and b is resultant from the slope of $\log(i)$ as a function of $\log(\nu)$.⁶ When b is 0.5 it indicates a diffusion-controlled process, and b value close to 1 corresponds to a surface-controlled process for the redox reactions. As depicted in **Fig. S7a**, b is 0.64 for Co-FLF satisfying a capacitive behaviour. To further determine the capacitive and diffusive contribution ratios, the following equations can be employed.

$$i = k_1\nu + k_2\nu^{1/2} \quad (\text{Equation S7})$$

where i , ν , $k_1\nu$, and $k_2\nu^{1/2}$ illustrate the total current, scan rate, capacitive controlled current and diffusion controlled current respectively. The capacitive contribution at different scan rates is depicted in **Fig. S7b**. The capacitive contribution from Co-FLF electrode of 64.11% at 20 mV s⁻¹ as depicted in **Fig. S7c**. Moreover, with the increase in scan rate from 5mV s⁻¹ to 50 mV s⁻¹

the capacitive contribution keeps increasing and reaches 80.45% at 50mV s⁻¹ indicating the fast electrochemical kinetics at higher scan rates.

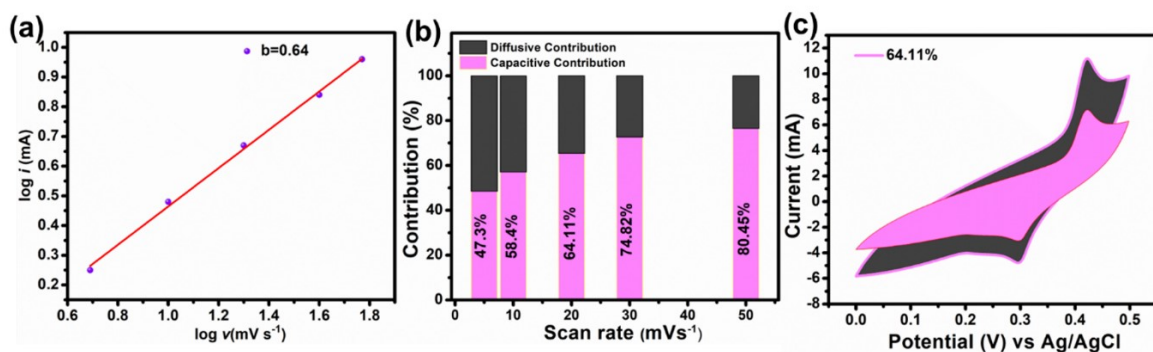


Fig. S7 (a) Log i (peak current) versus log v (scan rate) plots obtained from CV data. (b) Capacitive contributions at various CV scan rates. (c) CV curve with a capacitive contribution at 20 mV s⁻¹.

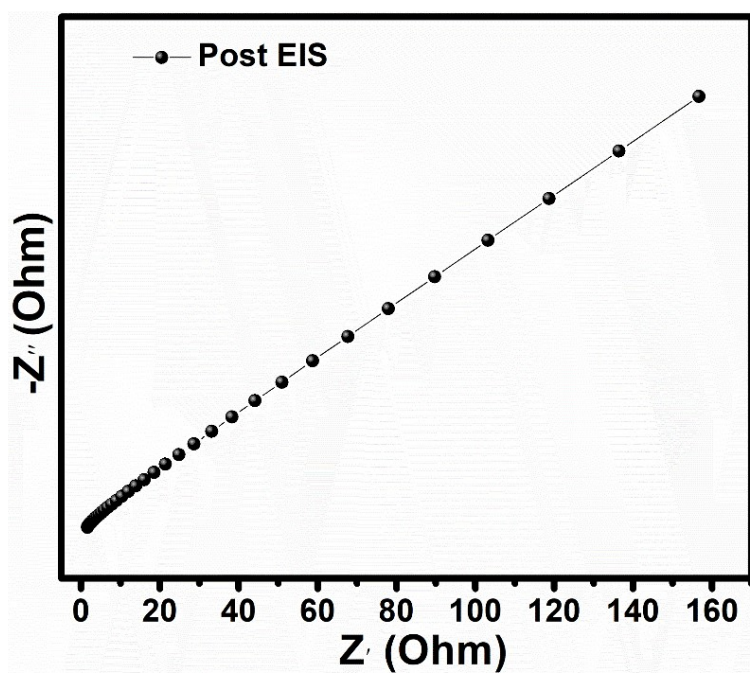


Fig. S8 Post stability EIS plot of Co-FLF.

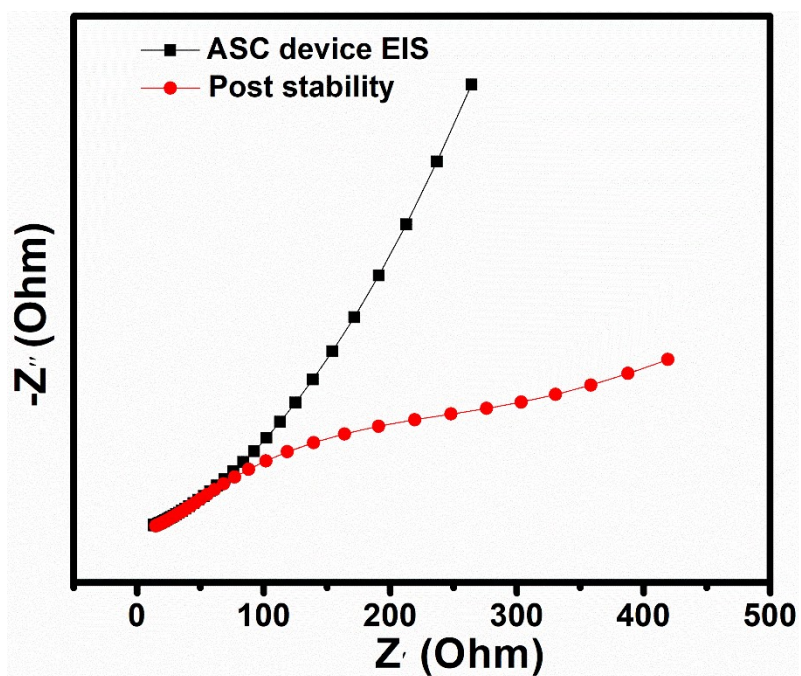


Fig. S9. ASC device EIS and Post stability EIS plot of ASC Device

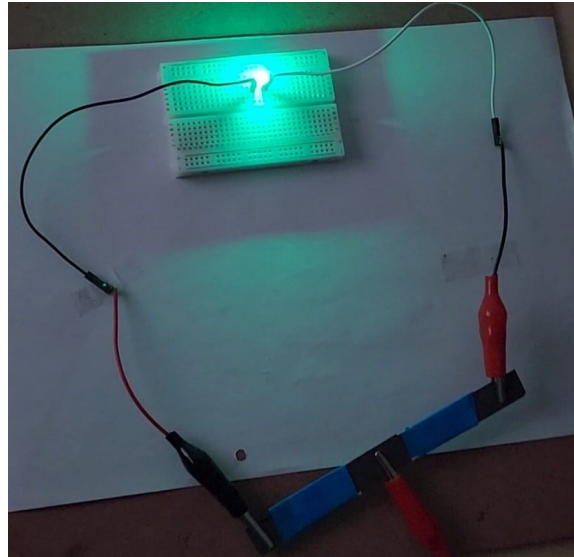


Fig. S10 Digital photograph of glowing LED after charging the ASC device.

Table S1. X-ray crystal structure data and refinement parameters of Co-FLF.

Identification code	Co-FLF
Empirical formula	C ₉ H ₆ Co _{0.50} F ₂ N ₂ O ₃
Formula weight	257.62
Crystal system	Triclinic
Space group	P -1
a (Å)	6.9776(12)
b (Å)	7.973(3)
c (Å)	9.575(2)
α (°)	79.20(3)
β (°)	70.959(19)
γ (°)	88.84(2)
V (Å ³)	494.2(2)
Z, d _{calcd} (mg m ⁻³)	2, 1.731
Temperature (K)	293(2)
Wavelength (Å)	0.71073
θ range	3.091 to 28.864
Goodness-of-fit (GOOF)	0.895
R ₁ , a wR ₂ b [I > 2σ(I)]	R ₁ = 0.0816, wR ₂ = 0.1662
R ₁ , a wR ₂ b (all data)	R ₁ = 0.1840, wR ₂ = 0.2228
Absorption correction	Semi-empirical from equivalents
Index ranges	-9<=h<=9, -10<=k<=10, -10<=l<=12
Crystal size (mm ³)	0.360 x 0.280 x 0.230
Refinement method	Full-matrix least-squares on F ²
Reflections collected / unique	3670 / 2177 [R(int) = 0.1594]
F (000)	259
CCDC no.	2441501

Table S2. Bond lengths (Å) and bond angles (°) for Co-FLF

Bond Lengths (Å)	
Co(1)-O(1)#1	2.124(4)
Co(1)-O(1)	2.124(4)
Co(1)-O(3)	2.141(4)
Co(1)-O(3)#1	2.141(4)
Co(1)-N(1)	2.219(6)
Co(1)-N(1)#1	2.219(6)
F(1)-C(3)	1.372(8)
F(2)-C(4)	1.364(8)
N(1)-C(5)	1.339(10)
N(1)-C(9)	1.350(9)
N(2)-N(2)#2	1.193(13)
N(2)-C(7)	1.508(10)
O(1)-C(1)	1.272(6)
O(2)-C(1)	1.256(8)
O(3)-H(3A)	0.8504
O(3)-H(3B)	0.8503
C(1)-C(2)	1.536(10)
C(2)-C(3)	1.382(10)
C(2)-C(4)#3	1.395(10)
C(3)-C(4)	1.400(11)
C(5)-C(6)	1.390(10)
C(5)-H(5)	0.9300
C(6)-C(7)	1.357(11)
C(6)-H(6)	0.9300
C(7)-C(8)	1.373(11)
C(8)-C(9)	1.421(10)
C(8)-H(8)	0.9300
C(9)-H(9)	0.9300

Bond Angles (°)	
O(1)#1–Co(1)–O(1)	180.0
O(1)#1–Co(1)–O(3)	88.91(17)
O(1)–Co(1)–O(3)	91.09(18)
O(1)#1–Co(1)–O(3)#1	91.09(17)
O(1)–Co(1)–O(3)#1	88.91(17)
O(3)–Co(1)–O(3)#1	180.0
O(1)#1–Co(1)–N(1)	91.7(2)
O(1)–Co(1)–N(1)	88.3(2)
O(3)–Co(1)–N(1)	88.17(19)
O(3)#1–Co(1)–N(1)	91.83(19)
O(1)#1–Co(1)–N(1)#1	88.3(2)
O(1)–Co(1)–N(1)#1	91.7(2)
O(3)–Co(1)–N(1)#1	91.83(19)
O(3)#1–Co(1)–N(1)#1	88.17(19)
N(1)–Co(1)–N(1)#1	180.0
C(5)–N(1)–C(9)	116.7(7)
C(5)–N(1)–Co(1)	120.1(6)
C(9)–N(1)–Co(1)	123.1(5)
N(2)#2–N(2)–C(7)	112.2(10)
C(1)–O(1)–Co(1)	131.1(5)
Co(1)–O(3)–H(3A)	109.6
Co(1)–O(3)–H(3B)	109.1
H(3A)–O(3)–H(3B)	104.5
O(2)–C(1)–O(1)	128.9(7)
O(2)–C(1)–C(2)	117.5(5)
O(1)–C(1)–C(2)	113.6(6)
C(3)–C(2)–C(4)#3	116.3(7)
C(3)–C(2)–C(1)	121.6(7)
C(4)#3–C(2)–C(1)	122.1(6)
F(1)–C(3)–C(2)	119.9(7)
F(1)–C(3)–C(4)	118.2(8)
C(2)–C(3)–C(4)	121.9(8)

F(2)–C(4)–C(2)#3	118.7(7)
F(2)–C(4)–C(3)	119.5(8)
C(2)#3–C(4)–C(3)	121.8(7)
N(1)–C(5)–C(6)	124.9(9)
N(1)–C(5)–H(5)	117.5
C(6)–C(5)–H(5)	117.5
C(7)–C(6)–C(5)	117.0(8)
C(7)–C(6)–H(6)	121.5
C(5)–C(6)–H(6)	121.5
C(6)–C(7)–C(8)	121.6(8)
C(6)–C(7)–N(2)	114.8(7)
C(8)–C(7)–N(2)	123.6(8)
C(7)–C(8)–C(9)	117.5(8)
C(7)–C(8)–H(8)	121.3
C(9)–C(8)–H(8)	121.3
N(1)–C(9)–C(8)	122.2(8)
N(1)–C(9)–H(9)	118.9
C(8)–C(9)–H(9)	118.9

Table S3. Supercapacitor performance of Co-FLF compared to other MOF based materials.

S.N O	Active materials	Electrolyte	Specific capacitance (F g ⁻¹)	Energy Density (Wh kg ⁻¹)	% Retention	Reference
1	Co-MOF	1 M KOH	446.8	13.70	88.3	[7]
2	S67/CC	KOH	8	3.25	91	[8]
3	Co-MOF derived Co ₃ O ₄	2 M KOH	226.1	26.6	97	[9]
4	Co-MOF	0.5 M LiOH	179.2	31.4	77.4	[10]
5	N-AC/Gr	6 M KOH	378.9	13.1	93	[11]
6	Co-MOF	6 M KOH	425	25.8	70	[12]
7	Co-NTA	3 M KOH	395	4.18	96.5	[13]
8	NiCo-MOF NSHS	3 M KOH	1126.7	20.94	65	[14]
9	Co ₉ S ₈ /NS	6 M KOH	734	14.85	96.5	[15]
10	Ni/Co-MOF	2 M KOH	758	20.9	75	[16]
11	Co-FLF	2M KOH	956	24.88	87.6	THIS WORK

References:

- 1 G. M. Sheldrick, *Acta Cryst A.*, 2008, **64**, 112–122.
- 2 G. Bergerhoff, M. Berndt and K. Brandenburg, *J Res Natl Inst Stand Technol.*, 1996, **101**, 221–225.
- 3 X. Liu, C. Shi, C. Zhai, M. Cheng, Q. Liu and G. Wang, *ACS Appl. Mater. Interfaces*, 2016, **8**, 4585–4591
- 4 Q. Yang, Q. Wang, Y. Long, F. Wang, L. Wu, J. Pan, J. Han, Y. Lei, W. Shi and S. Song, *Adv. Energy Mater.*, 2020, **10**, 1903193.
- 5 B. Long, M.-S. Balogun, L. Luo, W. Qiu, Y. Luo, S. Song and Y. Tong, *Adv. Energy Mater.*, 2018, **8**, 1701681.
- 6 Y. Qiao, J. He, Y. Zhou, S. Wu, X. Li, G. Jiang, G. Jiang, M. Demir and P. Ma, *ACS Appl. Mater. Interfaces.*, 2023, **15**, 52381–52391.
- 7 R. Rajak, M. Saraf, A. Mohammad and S. M. Mobin, *J. Mater. Chem. A.*, 2017, **5**, 17998–18011.
- 8 C.-Y. Xiao, T.-Y. Chen, R.-J. Chung, S. Yougbaré, L.-Y. Lin and Y.-F. Wu, *J. Energy Storage.*, 2022, **55**, 105622.
- 9 Y. Tao, Y. Wu, H. Chen, W. Chen, J. Wang, Y. Tong, G. Pei, Z. Shen and C. Guan, *Chem. Eng. J.*, 2020, **396**, 125364.
- 10 D. Y. Lee, D. V. Shinde, E.-K. Kim, W. Lee, I.-W. Oh, N. K. Shrestha, J. K. Lee and S.-H. Han, *Micropor Mesopor Mat.*, 2013, **171**, 53–57.
- 11 Q. Xie, R. Bao, A. Zheng, Y. Zhang, S. Wu, C. Xie and P. Zhao, *ACS Sustain. Chem. Eng.*, 2016, **4**, 1422–1430.
- 12 S. Khan, S. Halder, S. Chand, A. K. Pradhan and C. Chakraborty, *Dalton Trans.*, 2023, **52**, 14663–14675.
- 13 Y. Yan, P. Gu, S. Zheng, M. Zheng, H. Pang and H. Xue, *J. Mater. Chem. A.*, 2016, **4**, 19078–19085.
- 14 J. Sun, X. Yu, S. Zhao, H. Chen, K. Tao and L. Han, *Inorg. Chem.*, 2020, **59**, 11385–11395.
- 15 S. Zhang, D. Li, S. Chen, X. Yang, X. Zhao, Q. Zhao, S. Komarneni and D. Yang, *J. Mater. Chem. A.*, 2017, **5**, 12453–12461.
- 16 S. Gao, Y. Sui, F. Wei, J. Qi, Q. Meng, Y. Ren and Y. He, *J. Colloid Interface Sci.*, 2018, **531**, 83–90.